Available online at www.sciencedirect.com
ScienceDirect
Catalysis Today 131 (2008) 450–456
CATALYSIS TODAY
www.elsevier.com/locate/cattod

MgO-modified VO_x/SBA-15 as catalysts for the oxidative dehydrogenation of *n*-butane

Wei Liu [a], Suk Yin Lai [a], Hongxing Dai [a,b], Shuiju Wang [c], Haizhen Sun [c], Chak Tong Au [a,*]

[a] *Department of Chemistry, Centre for Surface Analysis and Research, Hong Kong Baptist University, Kowloon Tong, Hong Kong, China*
[b] *Laboratory of Catalysis Chemistry and Nanoscience, Department of Chemistry and Chemical Engineering, College of Environmental and Energy Engineering, Beijing University of Technology, Beijing 100022, China*
[c] *Chemistry and Chemical Engineering College, Xiamen University, Xiamen 361005, China*

Available online 26 November 2007

Abstract

VO_x catalysts supported on SBA-15 with and without MgO modification were prepared and characterized by N_2 adsorption–desorption, XRD, HRTEM, H_2-TPR, NH_3-TPD and XPS. Compared to the VO_x/SBA-15 catalyst, the VO_x/MgO/SBA-15 ones exhibit much higher C_4-olefins selectivity and yield in the oxidative dehydrogenation of *n*-butane. The enhanced performance can be attributed to the rise in VO_x reducibility as well as to the relatively lower acidity of the MgO-modified SBA-15 materials.

Keywords: Mesoporous SBA-15; Vanadium oxide; MgO modification; Oxidative dehydrogenation; *n*-Butane

1. Introduction

The global demand for C_4-olefins (1-butene, *cis*-2-butene, *trans*-2-butene and butadiene) increases in recent years. Since *n*-butane is relatively cheap and easy to get, much efforts have been devoted to the conversion of *n*-butane to C_4-olefins. Oxidative dehydrogenation (ODH) of *n*-butane is regarded as a promising method alternative to the classical non-oxidative dehydrogenation of *n*-butane [1]. The ODH reaction of *n*-butane is thermodynamically favorable and can proceed at a temperature much lower than that adopted in a non-oxidative manner [2]. To a certain extent, the conditions of ODH reaction lessen the problems of coke formation and catalyst deactivation. The ODH of *n*-butane has been extensively studied since 1967, and there are a number of review papers on the topic (e.g. [1,3–5]). The ODH reaction, however, is still hampered by the deep oxidation of *n*-butane and C_4-olefins to carbon oxides. Thus the fabrication of a selective catalyst for high C_4-olefins yield remains a challenge in catalysis.

Vanadium oxide supported on SiO_2 [6,7], Al_2O_3 [8–12] and MgO [13–24] has been found active and selective to the ODH of *n*-butane. The conversion of *n*-butane and selectivity to C_4-olefins depend greatly on the nature of vanadium oxides and their interaction with the support materials. It is generally accepted that well-dispersed VO_x is selective to the ODH reaction while a presence of V_2O_5 crystallites leads to deep oxidation products [6]. Another factor of concern is the acid–base character of the catalyst. C_4-olefins are considered to be basic and nucleohpilic due to their high electron densities at the π bonds. On basic oxides, C_4-olefins adsorption is not strong and selectivity is relatively high. On acidic oxides, they undergo strong adsorption and further oxidation to carbon oxides [22].

As far as the percentage yield (ca. 35%) of C_4-olefins is concerned, VO_x/MgO is the best supported catalyst for the ODH of *n*-butane. The outstanding performance has been related to the formation of magnesium orthovanadate [13] but the exact identity of the active phase is still under debate [23]. The discovery of novel materials such as MCM-41 and SBA-15 provides new routes for the fabrication of high-performance catalysts. Recently, Wei et al. reported the successful preparation of MgO-modified SBA-15 of large surface area,

* Corresponding author. Tel.: +852 3411 7067; fax: +852 3411 7348.
E-mail address: pctau@hkbu.edu.hk (C.T. Au).

0920-5861/$ – see front matter © 2007 Elsevier B.V. All rights reserved.
doi:10.1016/j.cattod.2007.10.054

and the results of CO_2-TPD showed that the MgO-modified material resembles MgO in basic strength [24]. In the present paper, we report for the first time the use of MgO-modified SBA-15 as support for VO_x catalysts. In terms of turnover rate, the VO_x/MgO/SBA-15 catalyst performs better than the VO_x/MgO catalyst in the ODH of *n*-butane. We investigated the physicochemical properties of the MgO-modified SBA-15 and the corresponding supported VO_x catalysts systematically by means of N_2 adsorption–desorption, XRD, HRTEM, XPS, H_2-TPR and NH_3-TPD techniques. The effect of MgO on the modification of acid characters of SBA-15 and VO_x/SBA-15 has been addressed.

2. Experimental

2.1. Preparation of VO_x supported on SBA-15 and MgO-modified SBA-15

The synthesis of SBA-15 [25] and MgO-modified SBA-15 [24] was carried out in acidic condition with P123 ($EO_{20}PO_{70}EO_{20}$, Aldrich) as template. The loading of VO_x (8.96 wt% V relative to SBA-15) on SBA-15 and on MgO-modified SBA-15 was by means of incipient wetness impregnation of the supports with a solution of ammonium metavanadate and oxalic acid (molar ratio 1:2) as described by Dai et al. [26]. First, a required amount of ammonium metavanadate (99%, Aldrich) and corresponding amount of oxalic acid dihydrate (99%, Aldrich) were dissolved in 4 ml deionized water. Then SBA-15 or MgO-modified SBA-15 powder was added and the mixture was dried at 120 °C overnight. The dried precursor was heated from room temperature (RT) to 600 °C at a rate of 1 °C/min and kept at this temperature for 5 h in air. The prepared catalysts are denoted as V/*x*Mg-SBA-15 (*x* represents molar ratio of Mg to V) and the corresponding MgO-modified SBA-15 are denoted as *x*Mg-SBA-15. For comparison purpose, the VO_x/MgO catalyst with 24 wt% V_2O_5 and 76 wt% MgO (denoted as 24VMgO) was also prepared according to the reported method [13].

2.2. Catalyst characterization

The BET surface areas and pore structures of the samples were measured on a Quantachrome NOVA-1200 instrument; prior to the adsorption of N_2 at −196 °C, the samples were degassed at 300 °C for 3 h. Powder X-ray diffraction investigation was conducted using a Rigaku diffractometer (Rigaku D-MAX) with Ni filtered Cu Kα radiation. The morphology of the catalyst was examined on a FEI TECNAI Field Emission HRTEM. The XPS investigation was conducted on a spectrometer equipped with a VG CLAM 4 MCD Analyzer and Mg Kα (1253.6 eV) radiation. The C 1s signal (284.6 eV) of contaminant carbon was used to calibrate the binding energies (BEs). The surface concentrations of elements were estimated on the basis of the corresponding peak areas being normalized using the Wagner Factor database.

In H_2 temperature-programmed reduction (H_2-TPR), 50 mg samples were used. The samples were first treated in dry air at 500 °C for 1 h and then cooled down to RT in N_2 (50 ml/min). The reduction was performed in the 100–800 °C range at a ramping rate of 10 °C/min in 5% H_2/Ar (50 ml/min). The effluent was monitored with a TCD detector.

NH_3 temperature-programmed desorption (NH_3-TPD) was carried out on the same instrument as H_2-TPR. In each experiment, we used 50 mg sample. After pretreatment in a flow of dry air (30 ml/min) at 500 °C for 1 h, the sample was exposed to NH_3 at RT for 30 min. The physically adsorbed NH_3 was removed by purging the sample with N_2 for 1 h. Then TPD was performed in N_2 flow (50 ml/min) at a heating rate of 10 °C/min, and the desorbed NH_3 was monitored by a TCD detector.

2.3. Catalytic evaluation

Catalytic tests for the ODH of *n*-butane were carried out at atmospheric pressure in a fixed-bed quartz tubular micro-reactor equipped with a coaxial thermocouple for temperature measurement. For each test, 0.2 g catalyst was introduced into the reactor. Each sample was first pressed into pellet and then crushed and sieved to particles in the range of 50–80 mesh. The feed was a mixture of *n*-butane, oxygen and nitrogen with a volume ratio of 4/8/88. The flow rate of the gases was controlled by mass flow controllers, and the total flow rate was 100 ml/min. The effluent was analyzed on-line by using a GC system (Shimadzu 8A). One GC equipped with FID detector and 0.19% picric acid/Carbograph column was used to separate hydrocarbons. The other GC equipped with TCD and columns of Porapak Q and molecular sieve 5 A was used to detect CO, CO_2 and O_2. Conversion of *n*-butane and selectivity to products was calculated based on the balance of carbon.

3. Results and discussion

3.1. Catalytic performance

The ODH reactions of *n*-butane with oxygen over the V/SBA-15, V/*x*Mg-SBA-15 and 24VMgO catalysts yield ethene and ethane (C_2), propene and propane (C_3), 1-butene (1-C_4), *cis*- and *trans*-2-butene (*c*-C_4 and *t*-C_4), 1,3-butadiene (1,3-C_4), carbon oxides (CO_x, i.e. CO and CO_2) and trace amount of *iso*butane. At 520 °C and a space velocity of 30,000 $cm^3\ h^{-1}\ g^{-1}_{cat}$, the V/SBA-15 catalyst shows a C_4-olefins selectivity of 27.3% at an *n*-butane conversion of 54.8% [27]. Under similar conditions in the absence of a catalyst, the conversion of *n*-butane is negligible. The presence of MgO has great effect on the conversion of *n*-butane and selectivity to C_4-olefins (Fig. 1 and Table 1). Over V/*x*Mg-SBA-15 (x = 0.71, 3.55, 4.97), conversions of *n*-butane are slightly higher than that over V/SBA-15. The initial rise in nominal Mg/V ratio caused an increase in *n*-butane conversion because there is the formation of well-dispersed tetrahedral VO_4 species on the MgO-modified SBA-15 sample. Further rise in nominal Mg/V ratio, however, resulted in a significant drop in surface area as well as the formation of polymeric VO_4 species and/or bulk Mg-vanadates; consequently, there was a decline in *n*-butane

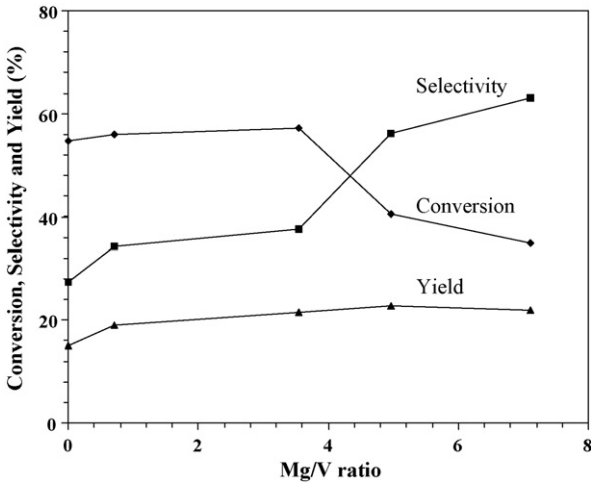

Fig. 1. *n*-Butane conversion, C_4-olefins selectivity, and C_4-olefins yield as a function of Mg/V ratio over the V/*x*Mg-SBA-15 catalysts.

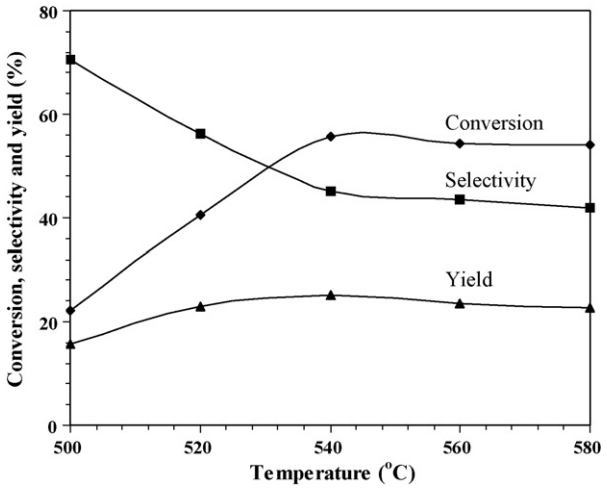

Fig. 2. *n*-Butane conversion, C_4-olefin selectivity, and C_4-olefin yield over V/4.97Mg-SBA-15 as a function of temperature.

conversion. The selectivity to C_4-olefins increases with MgO presence, the best yield (22.9%) of C_4-olefins was achieved at 520 °C over the V/4.97Mg-SBA-15 catalyst, with the corresponding C_4-olefins selectivity and *n*-butane conversion being 56.3 and 40.6%, respectively. The selectivity to CO_x decreased gradually from 67.8 to 34.9% when the nominal Mg/V ratio increased from 0 to 7.11. In order to get a better understanding of the effect of MgO doping on catalytic performance, we compared the selectivity to C_4-olefins at similar *n*-butane conversion and temperature over the V/SBA-15 and V/0.71Mg-SBA-15 catalysts. One can see that the selectivity to C_4-olefins was 17.2% over the former and 34.2% over the latter at 56% *n*-butane conversion and 520 °C. The results demonstrated that the introduction of MgO has a positive effect on the ODH reaction.

The effect of temperature on the catalytic performance of V/*x*Mg-SBA-15 was examined over the V/4.97Mg-SBA-15 catalyst in the 500–580 °C range (Fig. 2). Below 540 °C, conversion of *n*-butane increases and selectivity decreases with a rise in temperature. At temperature higher than 540 °C, conversion of *n*-butane and selectivity to C_4-olefins almost level off. The highest yield to C_4-olefins (25.1%) is at 540 °C.

Turnover frequencies (TOF) of C_4-olefins products over the V/SBA-15, 24VMgO and V/*x*Mg-SBA-15 catalysts have been calculated and compared as depicted in Table 1. The 24VMgO catalyst is higher than V/SBA-15 in TOF value. With MgO modification, significantly higher TOF values are obtained over the V/*x*Mg-SBA-15 catalysts. The TOF values over V/4.97Mg-SBA-15 and V/7.11Mg-SBA-15 is as high as 4.86×10^{-21} and 5.11×10^{-21} $\mu molC_4^=/V_{atom}$ S.

3.2. Characterization

3.2.1. Textural property

The N_2 adsorption–desorption of all the *x*Mg-SBA-15 samples are typical of Type-IV isotherm, indication of ordered mesoporous structure. The data of surface areas, pore volumes and pore sizes of the samples are summarized in Table 2. With the rise in Mg content, there is a gradual decrease in specific surface area and pore volume. Nevertheless, the 7.11Mg-SBA-15 samples with the highest Mg content still gives a respectable specific surface area of 296 m^2/g and pore volume of 0.54 ml/g. It is observed that the mesopore diameters of *x*Mg-SBA-15 remain the same (8.1 nm) due to the fact that in the *in situ* synthesis the pore size is determined solely by the size of the surfactant micelles. The average pore diameter increases with the Mg content and stabilizes at about 7 nm. The difference between mesopore diameter and average pore diameter is an

Table 1
Catalytic performance of V/SBA-15, V/*x*Mg-SBA-15 and 24VMgO at 520 °C and a space velocity of 30,000 $cm^3\ h^{-1}\ g^{-1}{}_{cat}$

Catalyst	Conversion (%)	Selectivity (%)							$C_4^=$Yield[b] (%)	TOF × 10^{21} ($\mu molC_4^=/V_{atom}$ S)
		1-C_4	*c*-C_4	*t*-C_4	1,3-C_4	CO	CO_2	$C_4^=$Dehy.[a]		
V/SBA-15[c]	54.8	5.7	5.5	6.9	9.2	56.1	11.7	27.3	15.0	2.45
V/0.71Mg-SBA-15	55.9	6.0	5.4	6.0	20.2	44.0	15.8	34.2	19.1	3.25
V/3.55Mg-SBA-15	57.2	6.9	4.6	5.5	26.2	40.6	15.8	37.6	21.5	4.26
V/4.97Mg-SBA-15	40.6	9.9	7.1	8.1	31.2	31.0	11.5	56.3	22.9	4.86
V/7.11Mg-SBA-15	34.8	15.2	8.8	8.5	36.4	23.4	11.5	63.0	22.0	5.11
24VMgO	67.6	6.3	6.0	8.3	13.6	30.4	19.9	44.0	29.7	2.79

[a] Selectivity to butenes and 1,3-butadiene.
[b] Yield to butenes and 1,3-butadiene.
[c] Data from Ref. [27].

Table 2
Physical properties of SBA-15, *x*Mg-SBA-15 and V/*x*Mg-SBA-15

Sample	S_{BET} (m^2/g)	*V* surface density (V/nm^2)	Pore volume (ml/g)	Mesopore diameter (nm)	Average pore diameter (nm)
SBA-15[a]	881	–	1.13	8.1	5.1
0.71Mg-SBA-15	766	–	1.03	8.1	5.4
3.55Mg-SBA-15	473	–	0.71	8.1	6.0
4.97Mg-SBA-15	354	–	0.64	8.1	7.2
7.11Mg-SBA-15	296	–	0.54	8.1	7.3
V/SBA-15[a]	540	1.7	0.76	7.2	7.2
V/0.71Mg-SBA-15	309	2.8	0.58	8.1	7.5
V/3.55Mg-SBA-15	254	3.0	0.50	7.2	7.9
V/4.97Mg-SBA-15	178	3.9	0.33	6.9	7.4
V/7.11Mg-SBA-15	65	9.8	0.15	6.0	9.2

[a] Data from Ref. [27].

indication of the existence of micropores [28–30]. With MgO modification, some of the Mg species can enter or block the micropores of SBA-15.

The loading of VO_x on *x*Mg-SBA-15 causes a further decrease in surface area and pore volume. With the nominal Mg/V ratio rising from 0 to 7.11, the reduction in surface area caused a gradual increase of vanadium surface density from 1.7 to 9.8 V/nm^2 (Table 2). However, the catalysts still display a kind of mesopore structure. At low contents of MgO modifier, the catalysts still retain a sort of Type-IV isotherm. Destruction of mesopore structure at high MgO contents is reflected on the surface area (Table 2) and BJH pore size distribution (not shown). For example, the V/7.11Mg-SBA-15 catalyst shows a surface area of below 100 m^2/g, and the pore size distribution curve is nearly flattened, reflecting the near complete elimination of mesopores. With the introduction of VO_x in

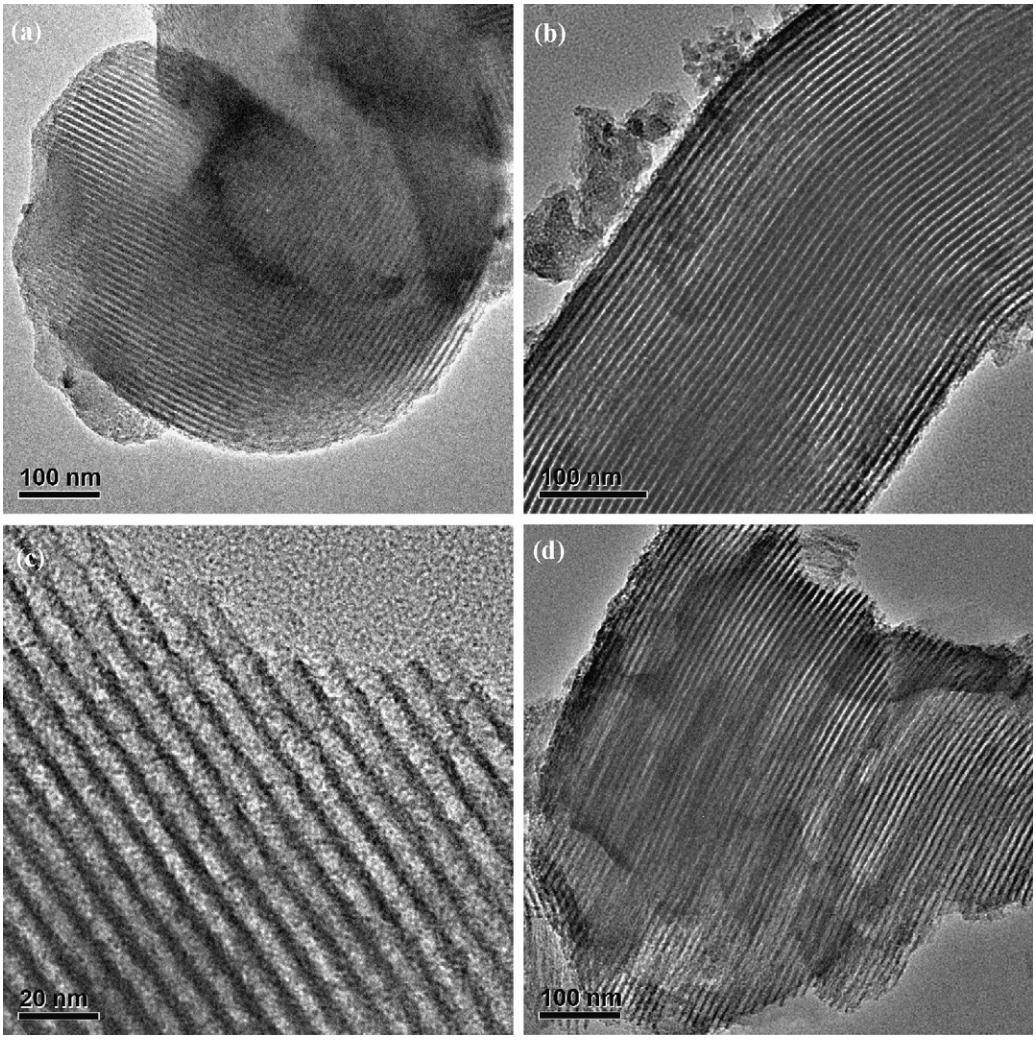

Fig. 3. TEM images of (a) 3.35Mg-SBA-15, (b, c) V/3.35Mg-SBA-15 and (d) V/SBA-15.

*x*Mg-SBA-15, there is a decrease in mesopore diameter. The average pore diameters of V/*x*Mg-SBA-15 are around 7.5 nm.

The TEM images of 3.35Mg-SBA-15, V/3.35Mg-SBA-15 and V/SBA-15 are shown in Fig. 3. One can see ordered pore channels in the three catalysts. From the image of 3.35Mg-SBA-15, one can see that the mouths of some mesopores are blocked by the large MgO particles located on the external surface of SBA-15, a situation which would cause a simultaneous decline in both pore volume and surface area. This is in accord with the surface area and pore volume results depicted in Table 2. From Fig. 3b and c, one can see that the mesopore structure is retained after the introduction of VO_x to 3.35Mg-SBA-15. Nevertheless, from the TEM images, one can see that there are more MgO particles located on the external surface. This could be caused by the acidic condition during the loading of VO_x and a certain amount of MgO originally inside the mesopores leaked out. Compared with the TEM images of V/SBA-15 (Fig. 3d), one can find that the addition of MgO can enhance the dispersion of VO_x. Relatively speaking, the V/SBA-15 sample shows more rod-like VO_x in the channels of the support than V/Mg-SBA-15. It is reckoned that the dispersion tendency of VO_x depends on the basicity of the support surface. On basic oxides, the dispersion of VO_x is secured by the interaction between MgO and VO_x and the interaction would be strong enough to stop the agglomeration of VO_x [31,32]. In other words, the presence of MgO with intrinsic basic character makes the Mg-SBA-15 a material better than SBA-15 for VO_x dispersion.

3.2.2. XRD

Shown in Fig. 4 are the small-angle XRD patterns of V/SBA-15 and V/*x*Mg-SBA-15 samples. The V/SBA-15 shows three well-resolved diffraction peaks at $2\theta = 0.90^\circ$, 1.75° and 2.08° attributable to (1 0 0), (1 1 0) and (2 0 0) diffraction, respectively. These diffraction peaks are also observed over the SBA-15 and *x*Mg-SBA-15 samples; the diffraction lines are characteristics of the hexagonal ordered structure of SBA-15 [25]. The loading of VO_x on *x*Mg-SBA-15 results in a decline in intensity and in the final disappearance of these three peaks.

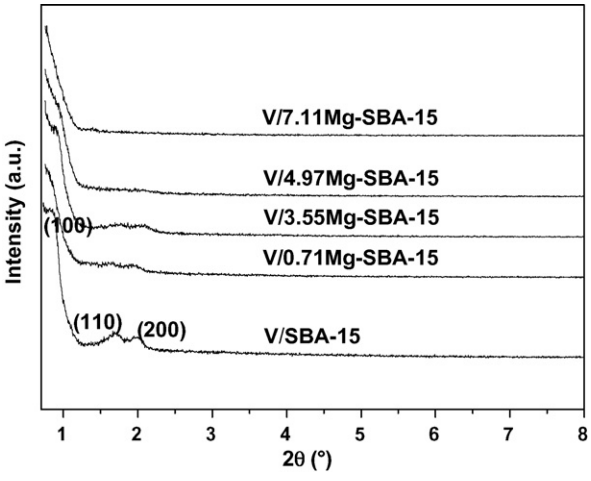

Fig. 4. Small-angle XRD patterns of V/SBA-15 and V/*x*Mg-SBA-15.

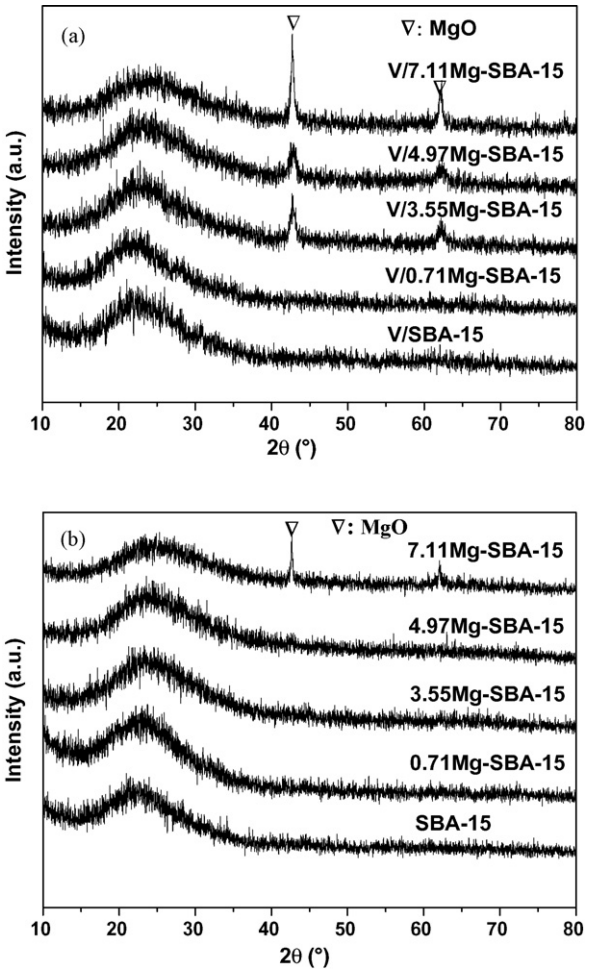

Fig. 5. Wide-angle XRD patterns of (a) V/SBA-15 and V/*x*Mg-SBA-15 and (b) SBA-15 and *x*Mg-SBA-15.

The results reflect the blockage of pores and the loss of long-range order of pore structure.

Fig. 5a shows the wide-angle XRD patterns of the V/SBA-15 and V/*x*Mg-SBA-15 samples. There are no peaks detected over V/SBA-15 and V/0.71Mg-SBA-15. With enhanced MgO presence, peaks of MgO crystallites appear, and with further increase in MgO, the peaks sharpen and rise in intensity. The results indicate that on V/*x*Mg-SBA-15, when *x* is equal to or bigger than 3.55, there is the formation of MgO crystallites that enlarge with an increase in *x* values. It is noted that only the 7.11Mg-SBA-15 would show MgO diffraction peaks. The results are in accord with the TEM observation that there is MgO leakage from the mesopores during the loading of VO_x. Despite there is a decrease in surface area, all the V/*x*Mg-SBA-15 samples do not show diffraction peaks of V_2O_5. The BET surface area of V/7.11Mg-SBA-15 is 65 m^2/g, much lower than that (123 m^2/g) of VO_x/SiO_2 of equal VO_x loading. We find that the former shows no diffraction peaks of V_2O_5 whereas the latter does. These results further confirm that the modification of SBA-15 with MgO results in better VO_x dispersion. We do not detect any diffraction peaks that can be related to magnesium vanadates over the V/*x*Mg-SBA-15 samples. The XRD results so far do not exclude the possible presence of

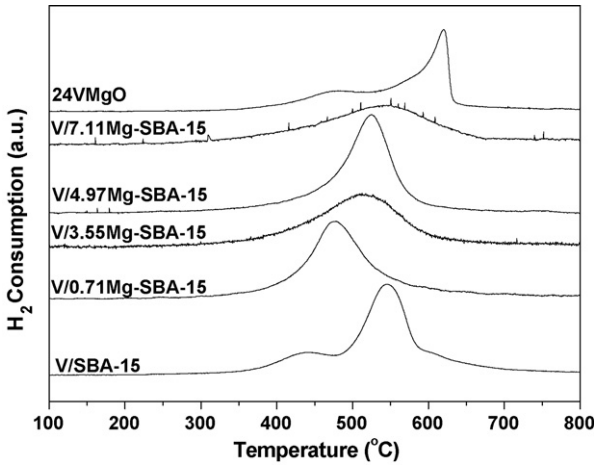

Fig. 6. TPR profiles of V/SBA-15 and V/*x*Mg-SBA-15.

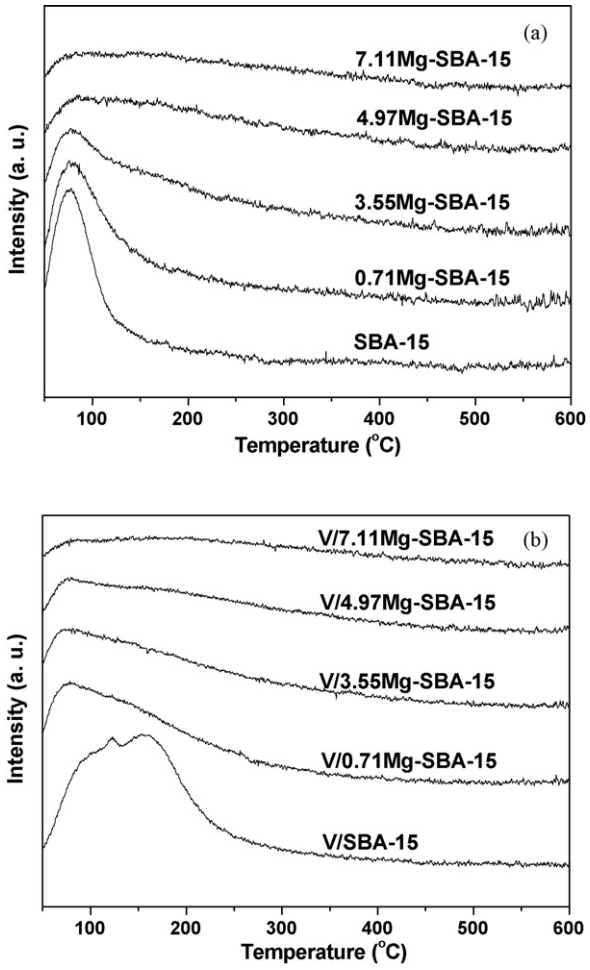

Fig. 7. NH_3-TPD profiles of (a) SBA-15 and *x*Mg-SBA-15 and (b) V/SBA-15 and V/*x*Mg-SBA-15.

magnesium vanadates. According to Chaar et al., magnesium vanadates could only be detected over V–Mg–O catalyst of high vanadium loading [13].

3.2.3. TPR

H_2-TPR spectra of V/SBA-15 and V/*x*Mg-SBA-15 are shown in Fig. 6. The V/SBA-15 sample shows two reduction peaks at 440 and 547 °C, respectively. The former can be attributed to the reduction of surface V ions with unsaturated coordination while the latter to the reduction of well-dispersed tetrahedral vanadium species [33]. The H_2-TPR spectrum of V/0.7Mg-SBA-15 shows only one peak at about 476 °C; the peak is assigned to the reduction of well-dispersed tetrahedral vanadium species. We propose that due to the dispersion effect of MgO or the formation of well-dispersed Mg-vanadate, the reduction of surface tetrahedral vanadium species occurs at much lower temperature (475 °C) over V/0.71Mg-SBA-15. Over V/3.55Mg-SBA-15 and V/4.97Mg-SBA-15, the reduction peak shifted to 512 and 525 °C, respectively, a temperature still lower than the reduction temperature of 547 °C over V/SBA-15. This could be a combined result of reduction in surface area and decline in VO_x dispersion. Further increase of MgO ($x = 7.11$) would result in peak broadening and a peak shift to ca. 550 °C. The 24VMgO sample showed two reduction peaks of vanadium species. The narrow peak that dominates at around 620 °C can be attributed to the reduction of $Mg_3(VO_4)_2$, because most of the vanadium species in 24VMgO are in the form of $Mg_3(VO_4)_2$ [2,16,34]. We tentatively suggest that there is the formation and aggregation of different magnesium vanadates on the surface over this catalyst. Apparently, despite the introduction of MgO caused an increase in vanadium surface density, due to the MgO dispersion effect, the V/*x*Mg-SBA-15 catalysts became more reducible. Based on the

Table 3
XPS results of V/SBA-15 and V/*x*Mg-SBA-15[b]

Catalyst	V 2 $p_{3/2}$ (eV)	O 1s (eV)	Surface atom ratio[a]		
			Mg/V	Mg/Si	Si/V
SBA-15	–	533.0	–	–	–
V/SBA-15	516.6	533.1	–	–	5.4 (9.5)
V/0.71Mg-SBA-15	517.2	532.7	2.2 (0.71)	0.5 (0.07)	4.3 (9.5)
V/3.55Mg-SBA-15	517.3	532.7	15.1 (3.55)	3.6 (0.37)	4.1 (9.5)
V/4.97Mg-SBA-15	517.3	532.0	18.4 (4.97)	5.1 (0.52)	3.6 (9.5)
V/7.11Mg-SBA-15	517.3	531.8	20.9 (7.11)	6.6 (0.75)	3.2 (9.5)
24VMgO	517.3	529.9	17.9 (7.14)	–	–

[a] The data were estimated based on the XPS results.
[b] The data in parentheses are bulk compositions (i.e. ratios based on nominal values).

H_2-TPR results, we conclude that the addition of MgO to VO_x/SBA-15 can enhance the reducibility of the catalysts.

3.2.4. NH_3-TPD

We studied the acid–base character of *x*Mg-SBA-15 and V/*x*Mg-SBA-15 by means of NH_3-TPD (Fig. 7). There is NH_3 desorption at about 77 °C over SBA-15 and *x*Mg-SBA-15. With the enhanced presence of MgO, the desorption peak weakens in intensity, indicating a decline in the number of acid sites. The loading of VO_x on SBA-15 results in the presence of new acid sites of stronger acidity which are reflected by the appearance of a NH_3 desorption peak at about 160 °C. With the presence of MgO, the sites of higher acidity is blocked first and the 160 °C desorption peak of V/*x*Mg-SBA-15 weakens and the 77 °C peak becomes dominant. At high enough MgO content, both desorption peaks decline due to the elimination of surface acidic sites. One can see that the modification of MgO can lower the acid strength of VO_x/SBA-15.

3.2.5. XPS

The XPS results are summarized in Table 3. The V $2p_{3/2}$ BEs of V/Mg-SBA-15 at about 517.3 eV is higher than that of VO_x/SBA-15 (516.6 eV). The rise in V $2p_{3/2}$ BEs can be attributed to the formation of Mg-vanadates in which the valence state of vanadium is 5+. BE of O 1s decreases gradually with the addition of MgO. For VO_x/SBA-15, O 1s BE is about 533.1 eV, close to that of SBA-15 (533.0 eV). At V/0.71Mg-SBA-15 and V/3.55Mg-SBA-15, O 1s BEs at 532.7 eV are slightly lower than that of VO_x/SBA-15. At higher loading of MgO, O 1s BE shifts towards that of MgO (530.0 eV). The surface Mg/V ratios are much larger than the nominal values. In other words, there is enrichment of MgO on the surface of the catalysts, which is a factor beneficial to the enhancement of C_4-olefins selectivity.

4. Conclusion

VO_x supported on MgO-modified SBA-15 has been prepared and tested as catalysts for the ODH of *n*-butane. The results of NH_3-TPD and TPR investigations demonstrated that with the introduction of MgO, there is a decrease in catalyst acidity and a rise in reducibility of the vanadia catalyst. This type of catalysts shows good selectivity to C_4-olefins at relatively high *n*-butane conversion. Over the V/4.97Mg-SBA-15 catalyst, the best result is 56.3% selectivity to C_4-olefins and 40.6% *n*-butane conversion at 520 °C and at a space velocity of 30,000 $cm^3\,h^{-1}\,g^{-1}_{cat}$. Compared to the 24VMgO catalyst, the V/*x*Mg-SBA-15 catalysts display much higher TOF values.

Acknowledgments

The work was supported by the Hong Kong Baptist University (FRG/06-07/II-10); the research activities conducted in BJUT was financed by the National Natural Science Foundation of PR China (Grant No. 20473006).

References

[1] E.A. Mamedov, V. Cortés Corberán, Appl. Catal. A 127 (1995) 1.
[2] M.A. Chaar, D. Patel, H.H. Kung, J. Catal. 109 (1988) 463.
[3] T. Blasco, J.M. López Nieto, Appl. Catal. A 157 (1997) 117.
[4] M.M. Bhasin, J.H. McCain, B.V. Vora, T. Imai, P.R. Pujadó, Appl. Catal. A 221 (2001) 397.
[5] L.M. Madeira, M.F. Portela, Catal. Rev. Sci. Eng. 44 (2002) 247.
[6] L. Owens, H.H. Kung, J. Catal. 144 (1993) 202.
[7] L. Owens, H.H. Kung, J. Catal. 148 (1994) 587.
[8] T. Blasco, A. Galli, J.M. López Nieto, F. Trifiró, J. Catal. 169 (1997) 203.
[9] J.M. López Nieto, P. Concepción, A. Dejoz, F. Melo, H. Knözinger, M.I. Vázquez, Catal. Today 61 (2000) 361.
[10] M.E. Harlin, V.M. Niemi, A.O.I. Krause, J. Catal. 195 (2000) 67.
[11] M.E. Harlin, V.M. Niemi, A.O.I. Krause, B.M. Weckhuysen, J. Catal. 203 (2001) 242.
[12] V.V. Chesnokov, A.F. Bedilo, D.S. Heroux, I.V. Mishakov, K.J. Klabunde, J. Catal. 218 (2003) 438.
[13] M.A. Chaar, D. Patel, M.C. Kung, H.H. Kung, J. Catal. 105 (1987) 483.
[14] J.M. López Nieto, A. Dejoz, M.I. Vázquez, W. O'Leary, J. Cunningham, Catal. Today 40 (1998) 215.
[15] A. Dejoz, J.M. López Nieto, F. Márquez, M.I. Vázquez, Appl. Catal. A 180 (1999) 83.
[16] C. Téllez, M. Menéndez, J. Santamaría, J. Catal. 183 (1999) 210.
[17] H.H. Kung, M.C. Kung, Appl. Catal. A 157 (1997) 105.
[18] C. Téllez, M. Abon, J.A. Dalmon, C. Mirodatos, J. Santamaría, J. Catal. 195 (2000) 113.
[19] A.A. Lemonidou, Appl. Catal. A 216 (2001) 277.
[20] O. Rubio, J. Herguido, M. Menéndez, Chem. Eng. Sci. 58 (2003) 4619.
[21] S.H. Ge, C.H. Liu, S.C. Zhang, Z.H. Li, Chem. Eng. J. 94 (2003) 121.
[22] T. Blasco, J.M. López Nieto, A. Dejoz, M.I. Vázquez, J. Catal. 157 (1995) 271.
[23] S. Albonetti, F. Cavani, F. Trifirò, Catal. Rev. Sci. Eng. 38 (1996) 413.
[24] Y.L. Wei, Y.M. Wang, J.H. Zhu, Z.Y. Wu, Adv. Mater. 15 (2003) 1943.
[25] D.Y. Zhao, J.L. Feng, Q.S. Huo, N. Melosh, G.H. Fredrickson, B.F. Chmelka, G.D. Stucky, Science 279 (1998) 548.
[26] H.X. Dai, A.T. Bell, E. Iglesia, J. Catal. 221 (2004) 491.
[27] W. Liu, S.Y. Lai, H.X. Dai, S.J. Wang, H.Z. Sun, C.T. Au, Catal. Lett. 113 (2007) 147.
[28] X.K. Li, W.J. Ji, J. Zhao, Z.B. Zhang, C.T. Au, J. Catal. 238 (2006) 232.
[29] S. Jun, S.H. Joo, R. Ryoo, M. Kruk, M. Jaroniec, Z. Liu, T. Ohsuna, O. Terasaki, J. Am. Chem. Soc. 122 (2000) 10712.
[30] R. Ryoo, C.H. Ko, M. Kruk, V. Antochshuk, M. Jaroniec, J. Phys. Chem. B 104 (2000) 11465.
[31] G. Deo, I.E. Wachs, J. Phys. Chem. 95 (1991) 5889.
[32] A. Corma, J.M. López Nieto, N. Paredes, M. Pórez, Y. Shen, H. Cao, S.L. Suib, Stud. Surf. Sci. Catal. 72 (1992) 213.
[33] F. Arena, F. Frusteri, G. Martra, S. Coluccia, A. Parmaliana, J. Chem. Soc., Faraday Trans. 93 (1997) 3849.
[34] A.A. Lemonidou, G.J. Tjatjopoulos, I.A. Vasalos, Catal. Today 45 (1998) 65.